Flow Past a Swept Wing with a Compliant Surface: Stabilizing the Attachment-Line Boundary Layer

By Leanne Allen and Thomas J. Bridges

Many aquatic species such as dolphins and whales have fins, which can be modeled as swept wings. Some of these fins, such as the dorsal fin of a dolphin, are semi-rigid and therefore can be modeled as a rigid swept wing with a compliant surface. An understanding of the hydrodynamics of the flow past swept compliant surfaces is of great interest for understanding potential drag reduction mechanisms, especially since swept wings are widely used in hydrodynamic and aerodynamic design. In this paper, the flow past a swept wing with a compliant surface is modeled by an attachment-line boundary layer flow, which is an exact similarity solution of the Navier–Stokes equations, flowing past a compliant surface modeled as an elastic plate. The hydrodynamic stability of the coupled problem is studied using a new numerical framework based on exterior algebra. The basic instability of the attachment line boundary layer on a rigid surface is a traveling wave instability that propagates along the attachment line, and numerical results show that the compliance results in a substantial reduction in the instability region. Moreover, the results show that, although the flow-field is three-dimensional, the qualitative nature of the instability suppression is very similar to the qualitative reduction of instability of the two-dimensional Tollmien–Schlichting modes in the classical boundary-layer flow past a compliant surface.

Address for correspondence: Thomas J. Bridges, Department of Mathematics and Statistics, University of Surrey, Guildford GU2 7XH, UK.

STUDIES IN APPLIED MATHEMATICS 110:333–349

Published by Blackwell Publishing, 350 Main Street, Malden, MA 02148, USA, and 9600 Garsington Road, Oxford, OX4 2DQ, UK.

1. Introduction

The fins on a wide range of aquatic species can be modeled as swept wings, and swept wings are now widely used on hydrodynamic vehicles as well as aerodynamic devices. On commercial aircraft, for example, the wings are swept in order to avoid shocks at higher cruising speed. The practical problem of designing these swept-back wings has led to the need for analysis of flow over a wing whose leading edge is not normal to the oncoming stream.

A schematic of the flow in the attachment-line region of a swept wing is shown in Figure 1. Experiments have shown that if transition occurs at some location on the attachment line, the outboard portion of the entire wing will rapidly become saturated with turbulent flow [2, 3]. Therefore any attempt to stabilize and prevent transition on a swept wing starts with the attachment-line boundary layer.

Theoretical and experimental results show that a small amount of suction on parts of the wing surface is very effective for laminar flow control (LFC) on swept wings (cf. [4] and discussion therein). In [4], it was shown that the basic three-dimensional attachment-line boundary-layer flow is susceptible to traveling wave disturbances that propagate along the attachment line. Recent work of Türkyilmazoğlu and Gajjar [5] have provided convincing numerical evidence that these instabilities are indeed propagating: they are convective rather than absolute instabilities. Neutral curves for these instabilities with and without the presence of steady suction are presented in [4] and show convincing agreement with experiments (see Figure 4 in [4]). The results also demonstrate that the attachment-line boundary layer can theoretically be stabilized with small amounts of suction.

On the other hand, for underwater vehicles, the use of compliant surfaces has been shown to be effective in promoting transition delay. For example, it

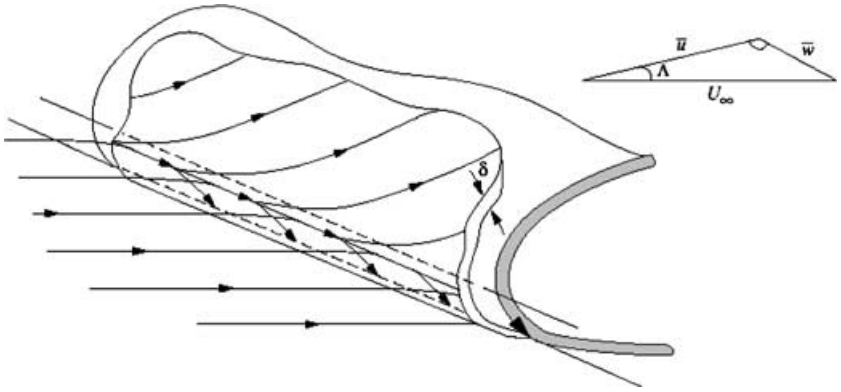

Figure 1. Schematic of the attachment-line boundary-layer flow on a swept wing [1].

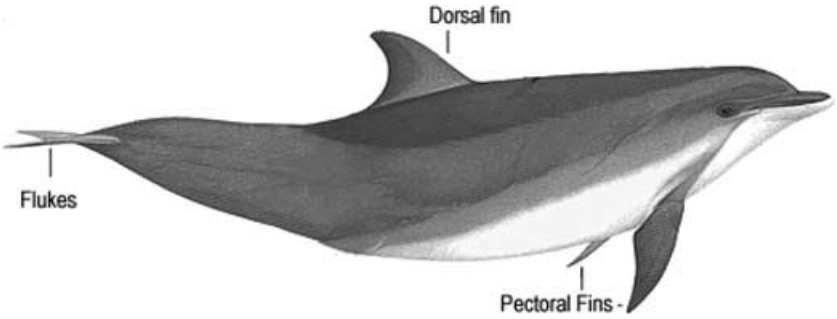

Figure 2. The swept-back fins of the dolphin.

is now widely established that compliance can have an effect on transition delay for two-dimensional boundary layers such as the Blasius boundary layer [6–10] and for three-dimensional boundary layers such as that on a rotating disc [11, 12]. Indeed, passive compliance has been proposed as a probable mechanism for the hydrodynamic efficiency of the dolphin [13–15].

However, as far as we are aware, the implications of surface compliance for transition on swept wings has never been studied.

The present paper takes its motivation from the dolphin, where evolution has molded the fin design in such a way that this swept wing attribute is evident on all three of its fin types. It can be seen in Figure 2 that the dorsal fin (the top fin used for balance), the pectoral fins (side fins which aid maneuvering), and caudral fin (propulsive lunate tail fluke) all resemble highly swept-back wings.

By neglecting end effects, a study of the infinite attachment line boundary layer adjacent to a compliant surface provides a basic model for flow past dolphin fins as well as swept wings with a compliant surface on underwater vehicles.

The paper of Hall et al. [4] is taken as a starting point. They showed that the non-parallel stability problem could be studied exactly using similarity variables, reducing the hydrodynamic stability problem to a sixth-order complex ordinary differential equation, which generalizes the Orr–Sommerfeld equation. They discovered that a wave traveling along the attachment line is the primary instability and presented neutral curves for a range of values of constant suction. Later work by Lin and Malik [16] used a larger class of stability perturbations but concluded that the modes discovered in [4] corresponded to the primary instability, occurring at the lowest Reynolds number. These linear stability results were further confirmed by Theofilis [17] using direct numerical simulation.

Here, the effect of compliance on the class of attachment-line instabilities discovered in [4] will be studied. The model for the wall is motivated by the properties of the dolphin. Historically, the skin of the dolphin was first studied in detail by Kramer [14], and was modeled theoretically by Carpenter and Garrad [6] as a membrane supported above a rigid flat plate by an

array of springs for use in a two-dimensional stability analysis of the Blasius boundary-layer flow past a compliant surface. This plate-spring model can be extended to three dimensions with isotropic elasticity properties in the two surface directions. In this paper, the Carpenter–Garrad model in three dimensions with anisotropy in the membrane surface, that is, differing flexural rigidity in the across-wing and spanwise directions, is used as a basis for the compliant surface model. Anisotropy in the direction normal to the skin surface can also be included in the model [8] but is not considered here.

The hydrodynamic stability problem is reduced to the sixth-order ODE eigenvalue problem of [4] but with boundary conditions determined by the compliant surface. The eigenvalue problem is solved numerically using a new exterior algebra framework [18]. This method generalizes the compound matrix method, and leads to an efficient and accurate method for stability problems on infinite or semi-infinite intervals.

The numerical results are quite surprising. Although the flowfield here is truly three-dimensional and the unstable traveling waves follow the attachment line and are transverse to the direction of the freestream, the effect of compliance is qualitatively very similar to that found for classical two-dimensional boundary layers. With an isotropic three-dimensional model for the compliant surface, the region of instability shrinks with increasing compliance.

In summary, the main new results in this paper are threefold: (a) it shows that compliance can have a substantial stabilizing effect on the predominant Tollmien–Schlichting-type mode associated with the flow over a swept wing; (b) it shows that the compound matrix method can be developed into a much more substantial and robust numerical method for hydrodynamic stability problems than previously thought; and (c) it shows the progress toward a theoretical analysis of the flow past dolphin fins.

2. The attachment-line boundary layer

The fluid is incompressible and viscous of kinematic viscosity ν, flowing adjacent to an infinite swept wing. The coordinates in the surface can be selected so that one of the coordinate directions is normal to the leading edge. Let y denote the dimensionless coordinate in the direction along the wing, x the other coordinate in the surface in the direction normal to the leading edge, and z the coordinate normal to the surface.

The governing equations for the fluid are the continuity equation and the Navier–Stokes equations. Denoting dimensional variables with a superscript $*$, the variables are non-dimensionalized as follows

$$x = \frac{x^*}{L_1}, \quad y = \frac{y^*}{L_1}, \quad z = \frac{x^*}{L_2}, \quad t = \frac{t^* V_0}{L_1}, \quad L_2 = \sqrt{\frac{\nu L_1}{U_0}},$$

$$u = \frac{u^*}{U_0}, \quad v = \frac{v^*}{V_0}, \quad w = \frac{w^* L_1}{U_0 L_2}, \quad p = \frac{p^*}{\rho V_0^2},$$

where L_2 represents the thickness of the boundary layer associated with the flow in the x–z plane. The dimensionless governing equations are

$$u_t + \gamma u u_x + v u_y + \gamma w u_z + \frac{1}{\gamma} p_x = \frac{\varepsilon}{Re}\left(u_{xx} + u_{yy} + \varepsilon^{-2} u_{zz}\right) \tag{1}$$

$$v_t + \gamma u v_x + v v_y + \gamma w v_z + p_y = \frac{\varepsilon}{Re}\left(v_{xx} + v_{yy} + \varepsilon^{-2} v_{zz}\right) \tag{2}$$

$$w_t + \gamma u w_x + v w_y + \gamma w w_z + \frac{1}{\gamma \varepsilon^2} p_z = \frac{\varepsilon}{Re}\left(w_{xx} + w_{yy} + \varepsilon^{-2} w_{zz}\right) \tag{3}$$

$$\gamma u_x + v_y + \gamma w_z = 0, \tag{4}$$

where

$$Re = \frac{V_0 L_2}{\nu}, \quad \gamma = \frac{U_0}{V_0}, \quad \text{and} \quad \varepsilon = \frac{L_2}{L_1}.$$

The basic state—the attachment-line boundary layer—is an exact solution of the Navier–Stokes equations [19] with a velocity field satisfying the boundary conditions

$$\begin{aligned} &u^* = v^* = 0, \quad w^* = W_0, \quad \text{at} \quad z^* = 0, \\ &u^* \to U_0 \frac{x^*}{L_1}, \quad v^* \to V_0, \quad \text{as} \quad z^* \to \infty. \end{aligned} \tag{5}$$

When $W_0 \neq 0$ there is a constant suction or blowing at the wall. In this paper, only the case $W_0 = 0$ is considered. The dimensionless mean velocity and pressure field take the form

$$u = x\overline{u}(z), \quad v = \overline{v}(z), \quad w = \overline{w}(z), \quad \text{and} \quad p = -\tfrac{1}{2}\gamma^2 x^2 + \overline{p}(z), \tag{6}$$

where $\overline{u}$, $\overline{v}$, $\overline{w}$, and $\overline{p}$ satisfy

$$\begin{aligned} \overline{u} + \overline{w}_z &= 0, \\ \overline{w}_{zzz} + \overline{w}_z^2 - \overline{w}\,\overline{w}_{zz} - 1 &= 0, \\ \overline{v}_{zz} - \overline{w}\,\overline{v}_z &= 0, \\ \overline{p} - \varepsilon^2 \gamma^2 \left(\overline{w}_z - \tfrac{1}{2}\overline{w}^2\right) &= \text{const}, \end{aligned} \tag{7}$$

with boundary conditions

$$\overline{w}_z(0) = 0, \quad \overline{w}(0) = 0, \quad \overline{w}_z(\infty) = -1, \quad \overline{v}(0) = 0, \quad \overline{v}(\infty) = 1.$$

The $\overline{w}$ component has the asymptotic property $\overline{w} \sim -[z - \delta]$ as $z \to \infty$, where the displacement, δ, is approximately 0.64790 [4].

Numerical expressions for the velocity field are obtained using expansion in terms of Chebyshev polynomials. The region $0 \leq z \leq z_\infty$, for some large value of z_∞, is mapped to $-1 \leq \tilde{z} \leq 1$ and then each velocity field is expanded in a finite series of Chebyshev polynomials, and the coefficients obtained numerically. Note that Chebyshev polynomials will *not* be used to solve the stability equations. The Chebyshev expressions yield very accurate values for the velocity field at arbitrary points in the interval $0 \leq z \leq z_\infty$ which are needed for input into the shooting algorithm for the stability problem.

3. Linearized hydrodynamic stability problem

In this section the linearized stability equations are derived following [4]. The disturbance velocity field in the x-direction varies linearly with x, with a periodic traveling wave structure for all components in the y-direction.

The instantaneous velocity field is decomposed into the basic and perturbed quantities as follows:

$$\begin{aligned} u(x, y, z, t) &= x\overline{u}(z) + x\,ReU(y, z, t) \\ v(x, y, z, t) &= \overline{v}(z) + V(y, z, t) \\ w(x, y, z, t) &= \overline{w}(z) + ReW(y, z, t) \\ p(x, y, z, t) &= -\frac{x^2}{2Re^2} + \overline{p}(z) + P(y, z, t), \end{aligned} \tag{8}$$

where U, V, W, and P represent the components of the disturbance. The polynomial x-dependence of the disturbance field reduces the linear stability equations to a system of ordinary differential equations (ODEs). The velocity and pressure fields (8) are substituted in the governing equations and linearized about the mean state. A normal-mode ansatz is then introduced: the perturbation field is taken to have a wave-like form traveling along the attachment line,

$$\begin{aligned} (U(y, z, t), V(y, z, t), W(y, z, t)) &= \mathrm{Re}\left\{(\widetilde{U}(z), \widetilde{V}(z), \widetilde{W}(z))e^{i\frac{\alpha}{\varepsilon}(y-ct)}\right\} \\ P(y, z, t) &= \mathrm{Re}\left\{\widetilde{P}(z)e^{i\frac{\alpha}{\varepsilon}(y-ct)}\right\}. \end{aligned} \tag{9}$$

A more general class of disturbances was considered by Lin and Malik [16], but they found that disturbances of the above form corresponded to the primary (i.e., lowest Reynolds number) instability.

Note that the pressure associated with the basic state has a polynomial dependence on x and therefore could drive a compliant surface even in the absence of the disturbance through the change in pressure in the streamwise direction. We will however not consider this effect here. This effect is similar to the linearly growing pressure field in plane channel flow with a compliant wall when the basic state is plane Poiseuille flow: it can either be ignored

or balanced by prescribed body forces in each wall (cf. [20], p. 210). Note that the polynomial x-dependence is also *transverse* to the wave disturbances which travel along the attachment line.

In summary, any motion of the compliant surface is taken to be due to the disturbance pressure field $P(y, z, t)$ in (8) only.

Substitution of the disturbance field into the Navier–Stokes equations linearized about the attachment line flow leads to the following set of ordinary differential equations

$$-i\alpha Rec\widetilde{U} + 2\overline{u}\widetilde{U} + i\alpha Re\overline{v}\widetilde{U} + \overline{w}\widetilde{U}_z + \widetilde{W}\overline{u}_z = \widetilde{U}_{zz} - \alpha^2\widetilde{U} \quad (10)$$

$$-i\alpha Rec\widetilde{V} + i\alpha Re\overline{v}\widetilde{V} + Re\overline{v}_z\widetilde{W} + \overline{w}\widetilde{V}_z + i\alpha Re\widetilde{P} = \widetilde{V}_{zz} - \alpha^2\widetilde{V} \quad (11)$$

$$-i\alpha Rec\widetilde{W} + i\alpha Re\overline{v}\widetilde{W} + \overline{w}\widetilde{W}_z + \overline{w}_z\widetilde{W} + Re\widetilde{P}_z = \widetilde{W}_{zz} - \alpha^2\widetilde{W}. \quad (12)$$

Similarly the continuity equation becomes

$$\widetilde{U} + i\alpha\widetilde{V} + \widetilde{W}_z = 0. \quad (13)$$

Now, by eliminating the pressure perturbation, $\widetilde{P}$ and the y-component of velocity V, we can systematically reduce Equations (10) to (12) to a pair of coupled ODEs to determine $\widetilde{U}$ and $\widetilde{W}$. The form of the disturbance pressure field is important for deriving the boundary conditions at the compliant surface, but the details are straightforward and not given here [21].

Define the operator $M \equiv (\frac{d^2}{dz^2} - \alpha^2)$, then the resulting pair of coupled equations to determine $\widetilde{U}$ and $\widetilde{W}$ are

$$(M + i\alpha Rec)\,\widetilde{U} = 2\overline{u}\widetilde{U} + \overline{u}_z\widetilde{W} + \overline{w}\widetilde{U}_z + i\alpha Re\overline{v}\widetilde{U}, \quad (14)$$

$$\begin{aligned}(M + i\alpha Rec)M\widetilde{W} = {} & i\alpha Re\overline{v}M\widetilde{W} - i\alpha Re\overline{v}_{zz}\widetilde{W} + \overline{w}M\widetilde{W}_z + \overline{w}_z M\widetilde{W} \\ & - 2(\overline{u}_z\widetilde{U} + \overline{u}\widetilde{U}_z) - (\overline{u}_{zz}\widetilde{W} + \overline{u}_z\widetilde{W}_z). \end{aligned} \quad (15)$$

The boundary conditions at $z = 0$ for a rigid wall are

$$\widetilde{U}(0) = \widetilde{W}(0) = \widetilde{W}'(0) = 0, \quad \text{at} \quad z = 0. \quad (16)$$

With appropriate asymptotic (large z) boundary conditions, the system (14) with boundary conditions (16) is the eigenvalue problem studied in [4].

The system (14) can be written as a coupled first-order system of six equations by defining new variables. Let $\mathbf{u} = (u_1, \ldots, u_6) \in \mathbb{C}^6$ have components defined by

$$\begin{aligned} u_1 = \widetilde{W} \quad u_2 = \widetilde{W}' \quad u_3 = \widetilde{W}'' \\ u_4 = \widetilde{W}''' \quad u_5 = \widetilde{U} \quad u_6 = \widetilde{U}'; \end{aligned}$$

then $\mathbf{u}$ satisfies the linear equation

$$\mathbf{u}_z = \mathbf{A}(z, \lambda)\mathbf{u}, \quad \mathbf{u} \in \mathbb{C}^6, \quad (17)$$

where $\mathbf{A}$ is the 6×6 matrix defined by

$$\mathbf{A}(z,\lambda) = \begin{pmatrix} 0 & 1 & 0 & 0 & 0 & 0 \\ 0 & 0 & 1 & 0 & 0 & 0 \\ 0 & 0 & 0 & 1 & 0 & 0 \\ -d(z) & -c(z) & b(z) & \overline{w} & -2\overline{u}_z & -2\overline{u} \\ 0 & 0 & 0 & 0 & 0 & 1 \\ \overline{u}_z & 0 & 0 & 0 & a(z) & \overline{w} \end{pmatrix} \tag{18}$$

with $\lambda = -i\alpha c$ and

$$\begin{aligned} a(z) &= \alpha^2 + i\alpha Re\overline{v} + \lambda Re + 2\overline{u} \\ b(z) &= 2\alpha^2 + \lambda Re + i\alpha Re\overline{v} + \overline{w}_z \\ c(z) &= \alpha^2\overline{w} + \overline{u}_z \\ d(z) &= \alpha^4 + \alpha^2\lambda Re + i\alpha^3 Re\overline{v} + \alpha^2\overline{w}_z + i\alpha Re\overline{v}_{zz} + \overline{u}_{zz}. \end{aligned}$$

Let $\mathbf{e}_1, \ldots, \mathbf{e}_6$ be the standard unit vectors in $\mathbb{C}^6$. Then the boundary conditions (16) can be written in the vector form

$$\langle \mathbf{e}_1, \mathbf{u} \rangle = \langle \mathbf{e}_2, \mathbf{u} \rangle = \langle \mathbf{e}_5, \mathbf{u} \rangle = 0 \quad \text{at} \quad z = 0.$$

where $\langle \cdot, \cdot \rangle$ is a standard Hermitian inner product on $\mathbb{C}^6$.

The form of the asymptotic ($z \to \infty$ boundary conditions) is deduced as follows. In [4] it is shown that the eigenfunctions for $\widetilde{U}$ and $\widetilde{V}$ have the asymptotic form

$$\widetilde{U} \sim e^{-\frac{1}{2}\widetilde{z}_\infty^2}, \quad \widetilde{W} \sim e^{-\alpha\widetilde{z}_\infty}, \quad \text{where } \widetilde{z}_\infty = z_\infty - 0.64790, \tag{19}$$

leading to the following proposed form for the boundary conditions to be applied at a large value of z, denoted z_∞:

$$\widetilde{W}' + \alpha\widetilde{W} = 0, \quad \widetilde{W}'' + \alpha\widetilde{W}' = 0, \quad \widetilde{U}' + z_\infty\widetilde{U} = 0 \quad \text{at} \quad z = z_\infty.$$

In vector form these boundary conditions are

$$\langle \mathbf{a}_1, \mathbf{u} \rangle = \langle \mathbf{a}_2, \mathbf{u} \rangle = \langle \mathbf{a}_3, \mathbf{u} \rangle = 0, \quad \text{at} \quad z = z_\infty, \tag{20}$$

with

$$\begin{aligned} \mathbf{a}_1 &= (\alpha, 1, 0, 0, 0, 0)^T \\ \mathbf{a}_2 &= (0, \alpha, 1, 0, 0, 0)^T \\ \mathbf{a}_3 &= (0, 0, 0, 0, z_\infty, 1)^T. \end{aligned} \tag{21}$$

4. Boundary conditions associated with the compliant surface

At the compliant surface, there are two kinematic conditions (ensuring the velocity of the compliant surface matches the velocity of the fluid adjacent to the surface) and a dynamic condition (in which the disturbance pressure field in the fluid drives the wall).

A sketch of the derivation of the boundary conditions at the wall is as follows. Let $\zeta^*(x, y, t)$ be the vertical displacement of the compliant surface. Then, to leading order in the displacements, the dimensional velocity field at the wall satisfies

$$u^* + \eta^* \frac{\partial u^*}{\partial z^*} + \cdots = 0 \quad \text{at} \quad z^* = 0,$$

$$v^* + \eta^* \frac{\partial v^*}{\partial z^*} + \cdots = 0 \quad \text{at} \quad z^* = 0,$$

$$w^* + \frac{\partial \zeta^*}{\partial t^*} + \cdots = 0 \quad \text{at} \quad z^* = 0.$$

Neglecting the higher-order terms, linearizing and nondimensionalizing leads to the following conditions:

$$ReU + \overline{u}_z \zeta = 0$$

$$V + \overline{v}_z \zeta = 0$$

$$\gamma ReW - \zeta_t = 0,$$

where ζ has been made dimensionless using L_2.

The governing equation for the wall displacement $\zeta^*(x, y, t)$ is taken to be

$$\rho_m b \frac{\partial^2 \zeta^*}{\partial t^{*2}} + d \frac{\partial \zeta^*}{\partial t^*} + \widetilde{B} \Delta_*^2 \zeta^* + 2\widetilde{B} \chi_1 \frac{\partial^4 \zeta^*}{\partial x^{*2} \partial y^{*2}} + \widetilde{B} \chi_2 \frac{\partial^4 \zeta^*}{\partial y^{*4}}$$
$$- T \Delta_* \zeta^* + k_E \zeta^* = -p^*_{\text{wall}} \tag{22}$$

where ρ_m is the surface density, b the surface thickness, d a damping parameter, $\widetilde{B}$ is the flexural rigidity in the x-direction, χ_1 and χ_2 are coefficients of anisotropy, T is the tension coefficient, Δ_* is the Laplacian in dimensional coordinates, k_E is a spring constant, and p^*_{wall} is the dimensional fluid pressure at the surface. After nondimensionalization and normal-mode substitution, the pressure at the wall takes the form

$$\widetilde{P}_{\text{wall}} = \frac{1}{\alpha^2 Re} \left(\widetilde{W}_{zzz} + \alpha^2 \widetilde{U} + \frac{\alpha^2}{c} \overline{v}_z \widetilde{W} \right) \Bigg|_{z=0}.$$

Equation (22) and the wall pressure field are a generalization to two (horizontal) space dimensions of the Kramer model for a compliant surface of Carpenter and Garrad [6].

Now, introducing a normal mode ansatz into (22), using the expression for $\widetilde{P}_{\text{wall}}$, the kinematic conditions, and the continuity equation, the boundary conditions at the wall can be expressed in the form

$$\begin{aligned}(\overline{u}_z(0) + i\alpha Re\overline{v}_z(0))\,\widetilde{W} + i\alpha Rec\widetilde{W}_z &= 0,\\ (i\alpha Re\overline{v}_z(0) + \overline{u}_z(0))\,\widetilde{U} + \overline{u}_z(0)\widetilde{W}_z &= 0,\\ ic(\widetilde{W}'''(0) + (\alpha^2 - i\alpha Re\, c)\widetilde{U}(0)) + \Gamma\widetilde{W}(0) &= 0,\end{aligned} \tag{23}$$

where

$$\begin{aligned}\Gamma = \alpha Re\big(\alpha^2 c^2 C_m + i\alpha c C_D - \alpha^4(1+\chi_2)C_{\widetilde{B}} - \alpha^2 C_T - C_{KE}\big)\\ + ic\overline{u}_z(0) + i\alpha^2\overline{v}_z(0).\end{aligned} \tag{24}$$

The boundary conditions for the two-dimensional case considered by Carpenter and Garrad [6] are recovered by neglecting the second equation, setting $\overline{v}_z(0) = 0$ in the first and third equation, and setting $\widetilde{U} = 0$ and $\chi_2 = 0$ in the third equation. The dimensionless coefficients C_m, C_D, etc., appearing in Γ represent wall properties and their definitions are exactly as in [6] with appropriate change for the length and velocity scales (see below for the expressions needed here).

Further details of the derivation of the above boundary conditions, including details of the anisotropic case and when the length and velocity scales differ in the various directions, can be found in [21].

Both C_T, the membrane tension parameter, and C_D, the damping parameter, are set equal to zero since earlier studies of the two-dimensional Blasius boundary layer revealed that these parameters appear not to have a significant effect on the instability region [18]. The expressions for C_m, $C_{\widetilde{\mathrm{B}}}$ and C_{KE} are derived much the same way as in [6] and [18]. The precise functional form for these parameters used in the numerics are

$$C_m = \frac{\rho_m}{\rho_e}\frac{b}{L_2} = \frac{\rho_m}{\rho_e}\frac{V_0 b}{\nu}\frac{1}{Re} = \frac{945}{1025}\frac{18(0.002)}{1.37\times10^{-6}}\frac{1}{Re} \approx \frac{24226.420899}{Re},$$

$$C_{\widetilde{B}} = \frac{\widetilde{B}}{\rho_e V_0^2 L_2^3} = \frac{\widetilde{B}V_0}{\rho_e \nu^3}\frac{1}{Re^3} \approx 6078227.413\frac{E}{Re^3},$$

$$C_{KE} = \frac{k_E L_2}{\rho_e V_0^2} = \frac{\nu k_E}{\rho_e V_0^3}Re \approx 2.291813\times10^{-13}(230ERe),$$

using the parameter values $\rho_m = 945$ kg m^{-3}, $\rho_e = 1025$ kg m^{-3}, $b = 0.002$ m, $V_0 = 18$ m s^{-1}, $\widetilde{B} = 8.9\times10^{-10}\,E$ N m, $\nu = 1.37\times10^{-6}$ m^2 s^{-1}, and $K_E = 230E$ suggested in [6] based on experiments.

The main parameter representing the wall is E, the wall rigidity, and it has units of NM^{-2}. An increase in E represents an increase in wall rigidity, with $E = \infty$ corresponding to a rigid wall.

The parameter χ_2 is defined by $\chi_2 = \frac{D_y}{D_x} - 1$, where D_y is the plate rigidity in the y-direction, and D_x is the plate rigidity in the x-direction. When $\chi_2 = 0$ the plate is isotropic in the surface directions. The parameter χ_2 can be used as a measure of anisotropy. In principle, it can be scaled out, using the identity $(1 + \chi_2)\widetilde{B} = D_y$ where D_y is the flexural rigidity in the y-direction. However, it may be useful to consider χ_2 and $\widetilde{B}$ as independent parameters, in order to get an idea of the effect of anisotropy on the linear stability of the coupled problem.

The three boundary conditions at the compliant surface can be written in standard vector form

$$\langle \mathbf{b}_1, \mathbf{u} \rangle = \langle \mathbf{b}_2, \mathbf{u} \rangle = \langle \mathbf{b}_3, \mathbf{u} \rangle = 0 \quad \text{at} \quad z = 0, \tag{25}$$

with

$$\begin{aligned} \mathbf{b}_1 &= (a_0, a_1, 0, 0, 0, 0)^T, \\ \mathbf{b}_2 &= (0, d_1, 0, 0, d_0, 0)^T, \\ \mathbf{b}_3 &= (b_0, 0, 0, b_3, b_4, 0)^T, \end{aligned} \tag{26}$$

where (replacing c with $c = i\lambda/\alpha$),

$$\begin{aligned} b_0 &= \Gamma \\ b_3 &= -\frac{\lambda}{\alpha} \\ b_4 &= -\frac{\lambda}{\alpha}(\alpha^2 + \lambda Re) \\ a_0 &= \overline{u}_z(0) + i\alpha Re \overline{v}_z(0) \\ a_1 &= -\lambda Re \\ d_0 &= \overline{u}_z(0) + i\alpha Re \overline{v}'(0) = a_0 \\ d_1 &= \overline{u}_z(0). \end{aligned}$$

These boundary conditions are well-posed if the vectors $\mathbf{b}_1$, $\mathbf{b}_2$, and $\mathbf{b}_3$ are linearly independent. For example, they are not linearly independent when $\lambda = 0$; in that case revised boundary conditions are necessary. For all the parameter values of interest here, these vectors are linearly independent.

In practice, the vector $\mathbf{b}_3$ is not used, but a scaled version is used:

$$\widetilde{\mathbf{b}}_3 = (1, 0, 0, \widetilde{b}_3, \widetilde{b}_4, 0)^T,$$

where $\widetilde{b}_3 = b_3/b_0$ and $\widetilde{b}_4 = b_4/b_0$. With this scaling, the boundary conditions for the rigid wall are obtained in the limit $E \to \infty$. We will be assuming b_0 is nonzero, which is generically satisfied, and is satisfied for all parameter values studied.

5. Numerics of the coupled stability problem

The numerical solution of the coupled eigenvalue problem is nontrivial because of the rapidly varying nature of the eigenfunctions. Previous numerical work for the rigid wall has been based predominantly on matrix methods. In [4] the Riccati method was also used but found to have numerical instabilities.

One of the main difficulties with matrix methods is that they create numerous spurious eigenvalues, because the domain truncation converts the continuous spectrum to a discrete spectrum with wildly oscillating eigenfunctions. This contamination of the spectrum leads to tedious accounting for real versus spurious eigenvalues, especially if a branch of continuous spectrum is unstable or nearly unstable. In [18] there is further discussion of this point, and in [22] there is an extreme example where a matrix (spectral) discretization creates an enormous number of unstable spurious eigenvalues.

The compound matrix method has features that make it highly desirable for eigenvalue problems, particularly on unbounded domains [23, 24]. Recently, the compound matrix method has been generalized in several directions [18]. The new developments of relevance here are: how to set up—even automate—the construction of the induced ODEs; how to set up boundary conditions at infinity including an algorithm for generating the starting vector, and how to set up the boundary conditions at $z = 0$.

The advantage of this approach is that it does not disturb the continuous spectrum, applies boundary conditions at infinity rigorously, preserves analyticity of the solutions, and maps a linear equation to a linear equation (in contrast to orthogonalization which transforms a linear equation to a nonlinear equation).

Let $\mathbf{e}_1, \ldots, \mathbf{e}_6$ be any orthonormal basis for $\mathbb{C}^6$ (without loss of generality this can be taken to be the standard basis). Then $\bigwedge^3(\mathbb{C}^6)$ is the vector space spanned by all nonzero elements of $\mathbf{e}_i \wedge \mathbf{e}_j \wedge \mathbf{e}_k$ where $\wedge$ is the wedge product. This space has dimension 20. This space is the appropriate one for studying the linear system (17) because the boundary conditions at $z = 0$ and $z = \infty$ define three-dimensional subspaces of $\mathbb{C}^6$.

The nonzero elements of $\mathbf{e}_i \wedge \mathbf{e}_j \wedge \mathbf{e}_k$ provide a basis for $\bigwedge^3(\mathbb{C}^6)$, and given this basis (with an assigned ordering) it is straightforward to construct the linear system on $\bigwedge^3(\mathbb{C}^6)$ induced from (17)

$$\mathbf{U}_z = \mathbf{A}^{(3)}(z, \lambda)\mathbf{U}, \quad \mathbf{U} \in \bigwedge^3(\mathbb{C}^6) \cong \mathbb{C}^{20}. \tag{27}$$

The induced matrix $\mathbf{A}^{(3)}(z, \lambda) : \bigwedge^3(\mathbb{C}^6) \to \bigwedge^3(\mathbb{C}^6)$ is a 20×20 matrix with entries, relative to the chosen basis,

$$\left\{\mathbf{A}^{(3)}\right\}_{i,j} = [\![\omega_i, \mathbf{A}\omega_j]\!]_3, \quad i, j = 1, \ldots, 20, \tag{28}$$

where $\omega_1 = \mathbf{e}_1 \wedge \mathbf{e}_2 \wedge \mathbf{e}_3$, $\omega_2 = \mathbf{e}_1 \wedge \mathbf{e}_2 \wedge \mathbf{e}_4$ and so on, using a lexical ordering. For any $\mathbf{U} = \mathbf{u}_1 \wedge \mathbf{u}_2 \wedge \mathbf{u}_3 \in \bigwedge^3(\mathbb{C}^6)$,

$$\mathbf{AU} \stackrel{\text{def}}{=} \mathbf{Au}_1 \wedge \mathbf{u}_2 \wedge \mathbf{u}_3 + \mathbf{u}_1 \wedge \mathbf{Au}_2 \wedge \mathbf{u}_3 + \mathbf{u}_1 \wedge \mathbf{u}_2 \wedge \mathbf{Au}_3,$$

and $[\![\cdot, \cdot]\!]_3$ is the induced inner product on $\bigwedge^3(\mathbb{C}^6)$,

$$[\![\mathbf{U}, \mathbf{V}]\!]_3 \stackrel{\text{def}}{=} \det \begin{bmatrix} \langle \mathbf{u}_1, \mathbf{v}_1 \rangle_{\mathbb{C}} & \langle \mathbf{u}_1, \mathbf{v}_2 \rangle_{\mathbb{C}} & \langle \mathbf{u}_1, \mathbf{v}_3 \rangle_{\mathbb{C}} \\ \langle \mathbf{u}_2, \mathbf{v}_1 \rangle_{\mathbb{C}} & \langle \mathbf{u}_2, \mathbf{v}_2 \rangle_{\mathbb{C}} & \langle \mathbf{u}_2, \mathbf{v}_3 \rangle_{\mathbb{C}} \\ \langle \mathbf{u}_3, \mathbf{v}_1 \rangle_{\mathbb{C}} & \langle \mathbf{u}_3, \mathbf{v}_2 \rangle_{\mathbb{C}} & \langle \mathbf{u}_3, \mathbf{v}_3 \rangle_{\mathbb{C}} \end{bmatrix}, \quad \mathbf{U}, \mathbf{V} \in \bigwedge^3(\mathbb{C}^6).$$

Details of this construction including how it can be automated are given in [18].

The strategy will be to integrate (27) from $z = z_\infty$ to $z = 0$. At $z = z_\infty$ the starting vector is constructed as follows. The three boundary conditions (20) define a three-dimensional subspace of $\mathbb{C}^6$. It is easy to check that this space is

$$\text{span}\{\mathbf{d}_1, \mathbf{d}_2, \mathbf{d}_3\} \quad \text{with} \quad \begin{cases} \mathbf{d}_1 = (1, -\alpha, \alpha^2, 0, 0, 0)^T \\ \mathbf{d}_2 = (0, 0, 0, 1, 0, 0)^T \\ \mathbf{d}_3 = (0, 0, 0, 0, 1, -z_\infty)^T. \end{cases}$$

The starting vector is then

$$\mathbf{U}(z_\infty) = \mathbf{d}_1 \wedge \mathbf{d}_2 \wedge \mathbf{d}_3,$$

which in terms of the standard basis for $\bigwedge^3(\mathbb{C}^6)$ becomes

$$\mathbf{U}(z_\infty) = (0, 0, 0, 0, 0, 0, 0, 1, -z_\infty, 0, 0, 0, 0, -\alpha, \alpha z_\infty, 0, \alpha^2, -\alpha^2 z_\infty, 0, 0)^T. \tag{29}$$

The starting vector can be taken to be any complex multiple of (29).

At $z = 0$ the requirement of satisfying the boundary conditions leads to a complex analytic function of the form

$$D(\lambda) = \langle \mathbf{F}(\lambda), \mathbf{U}(0, \lambda) \rangle_{\mathbb{R}^{20}}, \tag{30}$$

where $\mathbf{F}(\lambda) \in \bigwedge^3(\mathbb{C}^6)$ represents the boundary conditions and the inner product is a *real* inner product on $\mathbb{R}^{20}$ (if a complex inner product is used, we replace $\mathbf{F}(\lambda)$ by $\overline{\mathbf{F}(\lambda)}$).

The element $\mathbf{F}(\lambda)$ is deduced from

$$\mathbf{F}(\lambda) = \mathbf{b}_1(\lambda) \wedge \mathbf{b}_2(\lambda) \wedge \widetilde{\mathbf{b}}_3(\lambda),$$

which can be expressed in terms of the basis for $\bigwedge^3(\mathbb{C}^6)$ as follows:

$$\begin{aligned} \mathbf{b}_1 \wedge \mathbf{b}_2 \wedge \widetilde{\mathbf{b}}_3 &= (a_0\mathbf{e}_1 + a_1\mathbf{e}_2) \wedge (\mathbf{e}_1 + \widetilde{b}_3\mathbf{e}_4 + \widetilde{b}_4\mathbf{e}_5) \wedge (d_0\mathbf{e}_5 + d_1\mathbf{e}_2) \\ &= a_0\widetilde{b}_3 d_0(\mathbf{e}_1 \wedge \mathbf{e}_4 \wedge \mathbf{e}_5) - a_0\widetilde{b}_3 d_1(\mathbf{e}_1 \wedge \mathbf{e}_2 \wedge \mathbf{e}_4) \\ &\quad - a_0\widetilde{b}_4 d_1(\mathbf{e}_1 \wedge \mathbf{e}_2 \wedge \mathbf{e}_5) - a_1 d_0(\mathbf{e}_1 \wedge \mathbf{e}_2 \wedge \mathbf{e}_5) \\ &\quad + a_1\widetilde{b}_3 d_0(\mathbf{e}_2 \wedge \mathbf{e}_4 \wedge \mathbf{e}_5), \end{aligned}$$

where, taking the standard lexical ordering for the basis, leads to the representation in $\mathbb{C}^{20}$,

$$\mathbf{F}(\lambda) = (0, -a_0\tilde{b}_3 d_1, -(a_0\tilde{b}_4 d_1 + a_1 d_0), 0, 0, 0, 0, a_0\tilde{b}_3 d_0, 0, 0, 0, 0, 0, a_1\tilde{b}_3 d_0, 0, 0, 0, 0, 0, 0)^T.$$

The numerical strategy is to integrate (27) from $z = z_\infty$ to $z = 0$, with Re, α, λ, and the wall parameters fixed, taking (29) as the starting vector. The numerical method used is an implicit Gauss–Legendre Runge–Kutta (GLRK) method, which has excellent preservation properties for quadratic invariants and equations in the form (27) have a family of quadric surfaces that must be preserved [18].

If $D(\lambda) = 0$ we have found an eigenvalue. If $D(\lambda) \neq 0$, Newton's method is used to iterate till $D(\lambda) = 0$ to machine precision. The results presented here are computed using $z_\infty = 10.0$ and the second-order implicit GLRK method.

6. Effect of compliance on the attachment line boundary layer

Curves of neutral stability represent in the clearest way the effect of parameters on hydrodynamic stability. Here the neutral stability curves, corresponding to $\mathrm{Re}(\lambda) = 0$ (equivalently $\mathrm{Im}(c) = 0$), will be presented in the α–Re plane. Values of the parameters corresponding to the inside of the thumb-shaped curve correspond to unstable perturbations and outside the curve they are stable.

Figure 3 shows the computed effect of wall rigidity on the neutral curves. When E is very large, the computed neutral curve for the attachment line boundary layer over a rigid flat plate is recovered. The computed values corresponding to the nose of the rigid-wing neutral curve are $Re\,(\mathrm{crit}) = 583.1$ with wavenumber $\alpha = 0.287855$ and wave speed $c_r = 0.382480$. These values agree very closely with those reported in [4], p. 239.

Compliance has a dramatic effect on the neutral curve as evidenced in Figure 3. The instability region is reduced in size and eventually bifurcates into two distinct regions. This effect is similar to that obtained by the addition of a flexible surface in the two-dimensional Blasius flow problem; see Figure 11 on page 498 of [6] and Figure 1 of [18].

Figure 4 shows a blowup of the region near the nose of the neutral curve as E approaches E_c. The point E_c, which we compute to be $E_c = 0.01236$, $Re \approx 683.5$, is the point where the neutral curve collapses to a point. For $E < E_c$ the attachment line instability is completely suppressed for all but very large Reynolds numbers. It should however be noted that the surface with $E = E_c$ is far from rigid, and therefore the system might be susceptible to wall instabilities. Nevertheless, the results do show a strong positive effect of compliance on stability, comparable to the effect of compliance on the flat plate boundary layer.

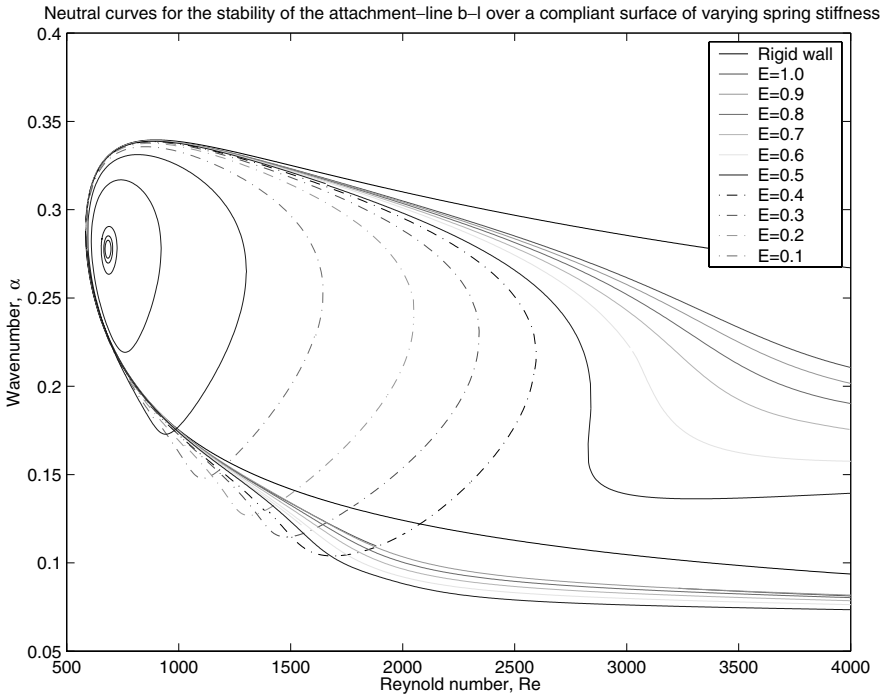

Figure 3. Effect of varying E on the neutral curves, plotted in the α–Re plane, with values inside a curve corresponding to instability.

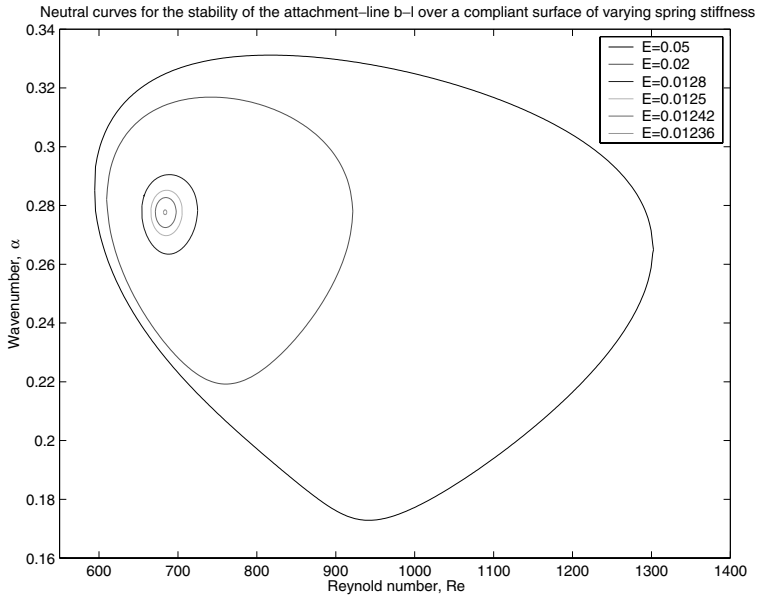

Figure 4. Blowup of the nose of the neutral curve in Figure 3 near the critical value of E.

7. Concluding remarks

The effect of compliance on the attachment-line boundary layer has been considered. The results show a clear indication that passive compliance can lead to stabilization of the coupled fluid-surface system. The effect is very similar to the stabilization of the Blasius boundary layer flow over a compliant surface. This shows that the effect of passive compliance is similar for two very different flowfields. This is promising because any underwater vehicle—or aquatic species—is composed of various parts all of which will have to contribute to the overall drag budget.

The model for a swept wing with a compliant surface is a simple one, and there are directions one could take to improve it. First, there are end effects. Secondly, it is clear from Figure 2 that the sweep angle varies along the chord of the fin on dolphins.

For the rigid wing, a weakly nonlinear analysis shows that the bifurcation at the nose is subcritical; see [25] for a weakly nonlinear analysis and [17] for the DNS point of view. With the dramatic effect of compliance on the form of the neutral curve, a natural question is what effect compliance has on the weakly nonlinear behavior: will it change the subcritical bifurcation to a supercritical bifurcation?

Finally, there is an interesting mathematical difficulty that arises in the analysis of the linear stability problem. The matrix $\mathbf{A}(z, \lambda)$ in (18) is asymptotic for large z to a polynomial function of z; that is, there exists $\sigma > 0$ such that

$$\lim_{z\to\infty} e^{\sigma z}\|\mathbf{A}(z, \lambda) - \mathbf{A}_0(\lambda) - z\mathbf{A}_1(\lambda)\| = 0.$$

When $\mathbf{A}_1(\lambda) = 0$, there is a rigorous theory for asymptotic boundary conditions. However, the z-term changes the nature of the problem. There is every reason to believe that (19) is exact or close to exact, but a theoretical justification of the large z boundary conditions would be of great interest.

References

1. W. H. Wentz, Jr., A. Ahmed, and R. Nyenhuis, Future results of natural laminar flow flight test experiments, *General Aviation Aircraft Aerodynamics*, SAE SP-621, pp. 37–50, 1985.
2. M. Gaster, On the flow along swept leading edges, *Aeronaut. Q.* 18:165–184 (1967).
3. D. I. A. Poll, Transition in the infinite swept attachment line boundary layer, *Aeronaut. Q.* 30:607–628 (1979).
4. P. Hall, M. R. Malik, and D. I. A. Poll, On the stability of an infinite swept attachment line boundary layer, *Proc. R. Soc. London A.* 395:229–245 (1984).
5. M. Türkyilmazoğlu and J. S. B. Gajjar, On the absolute instability of the attachment line and swept-Hiemenz boundary layers, *Theor. Comput. Fluid Dyn.* 13:57–75 (1999).
6. P. W. Carpenter and A. D. Garrad, The hydrodynamic stability of flow over Kramer-type compliant walls: Part 1. Tollmien–Schlichting instabilities, *J. Fluid Mech.* 155:465–510 (1985).

7. P. W. Carpenter, Status of transition delay using compliant walls, in *Viscous Drag Reduction in Boundary Layers*, Vol. 123 (D. M. Bushell and J. N. Hefner, Eds.), *Progress in Astro. & Aero., AIAA*, 79–113, 1990.
8. P. W. Carpenter and P. J. Morris, The effects of anisotropic wall compliance on boundary-layer stability and transition, *J. Fluid Mech.* 218:171–223 (1990).
9. A. D. Lucey and P. W. Carpenter, Boundary layer instability over compliant walls: Comparison between theory and experiment, *Phys. Fluids* 7:2355–2363 (1995).
10. C. Davies and P. W. Carpenter, Numerical simulation of the evolution of Tollmien-Schlichting waves over a finite panel, *J. Fluid Mech.* 335:361–392 (1997).
11. A. J. Cooper and P. W. Carpenter, The stability of rotating-disc boundary-layer flow over a compliant wall: Part 1. Type I and II instabilities, *J. Fluid Mech.* 350:231–259 (1997).
12. A. J. Cooper and P. W. Carpenter, The stability of rotating-disc boundary-layer flow over a compliant wall: Part 2. Absolute instabilities, *J. Fluid Mech.* 350:261–270 (1997).
13. M. O. Kramer, The dolphin's secret, *New Sci.* 7:1118–1120 (1960).
14. M. O. Kramer, Hydrodynamics of the dolphin, *Adv. Hydrosci.* 2:111–130 (1965).
15. P. W. Carpenter, C. Davies, and A. D. Lucey, Hydrodynamics and compliant walls: Does the dolphin have a secret? *Curr. Sci.* 79:758–765 (2000).
16. S. R. Lin and M. R. Malik, On the stability of attachment-line boundary layers: Part 1. The incompressible swept Hiemenz flow, *J. Fluid Mech.* 311:239–255 (1996).
17. V. Theofilis, On linear and nonlinear instability of the incompressible swept attachment line boundary layer, *J. Fluid Mech.* 355:193–227 (1999).
18. L. Allen and T. J. Bridges, Numerical exterior algebra and the compound matrix method, *Numer. Math.* 92:197–232 (2002).
19. L. F. Crabtree, D. Küchemann, and L. Sowerby, Three-dimensional boundary layers, in *Laminar Boundary Layers* (L. Rosenhead, Ed.,), pp. 409–488, Oxford University Press, Oxford, 1963.
20. C. Davies and P. W. Carpenter, Instabilities in a plane channel flow between compliant walls, *J. Fluid Mech.* 352:205–243 (1997).
21. L. Allen, Modelling dolphin hydrodynamics: The numerical analysis & hydrodynamic stability of flow past compliant surfaces, Ph.D. Thesis, University of Surrey, 2001.
22. I. V. Barashenkov and E. V. Zemlyanaya, Oscillatory instabilities of gap solitons: A numerical study, *Comput. Phys. Commun.* 126:201–244 (2000).
23. B. S. Ng and W. H. Reid, An initial value method for eigenvalue problems using compound matrices, *J. Comput. Phys.* 30:125–136 (1979).
24. B. S. Ng and W. H. Reid, The compound matrix method for ordinary differential equations, *J. Comput. Phys.* 58:209–228 (1985).
25. P. Hall and M. R. Malik, On the instability of a three-dimensional attachment-line boundary layer: Weakly nonlinear theory and a numerical approach, *J. Fluid Mech.* 163:257–282 (1986).

University of Surrey

(Received May 1, 2002)